

Article

Not peer-reviewed version

Heat Transfer in Composite Cylinders Under Harmonically Oscillating Ambient Conditions

[Rajai S. Alassar](#)*, [Mohammed Abushoshah](#), [Husain Al-Attas](#), [Said Al Algarni](#)

Posted Date: 23 March 2026

doi: 10.20944/preprints202603.1665.v1

Keywords: composite cylinder; conduction; Biot; oscillation; Duhamel's principle



Preprints.org is a free multidisciplinary platform providing preprint service that is dedicated to making early versions of research outputs permanently available and citable. Preprints posted at Preprints.org appear in Web of Science, Crossref, Google Scholar, Scilit, Europe PMC.

Copyright: This open access article is published under a [Creative Commons CC BY 4.0 license](#), which permit the free download, distribution, and reuse, provided that the author and preprint are cited in any reuse.

Disclaimer/Publisher's Note: The statements, opinions, and data contained in all publications are solely those of the individual author(s) and contributor(s) and not of MDPI and/or the editor(s). MDPI and/or the editor(s) disclaim responsibility for any injury to people or property resulting from any ideas, methods, instructions, or products referred to in the content.

Article

Heat Transfer in Composite Cylinders Under Harmonically Oscillating Ambient Conditions

Rajai S. Alassar *, Mohammed Abushoshah, Husain Al-Attas and Said Al Garni

King Fahd University of Petroleum & Minerals, Department of Mathematics, Interdisciplinary Research Center for Sustainable Energy Systems, Dhahran 31261, Saudi Arabia

* Correspondence: alassar@kfupm.edu.sa; Tel.: +966138602787

Abstract

An analytical solution is presented for transient heat conduction in a two-layer composite cylinder subjected to outer-surface convection with a general time-dependent ambient temperature. Using Duhamel's principle, closed-form series expressions are derived and then specialized to harmonic ambient fluctuations, recovering the classical constant-ambient solution in the zero-frequency limit. A parametric study shows that the ratio of the inner layer conductivity to the conductivity of the outer layer strongly shapes interfacial gradients and mean-temperature evolution, with sensitivity concentrated at small ratios and diminishing when the ratio is larger than 0.1. Increasing Biot number accelerates the heat transfer and approaches the isothermal-surface limit as it becomes extremely large. The geometric aspect ratio is most influential when the inner layer is resistive, and becomes weak for large conductivity ratio, supporting thin-coating approximations. Under harmonic ambient fluctuations, the response rapidly reaches a periodic steady state; higher frequency decreases amplitude and increases phase lag, while larger Biot numbers amplify oscillations and reduce delay. The coupled effects of the aspect ratio and the conductivity ratio govern penetration and phase behavior.

Keywords: composite cylinder; conduction; Biot; oscillation; Duhamel's principle

Introduction

Concentric, multi-layer cylinders arise whenever a cylindrical component must simultaneously carry load and manage heat, for example, a metallic pipe protected by an insulating jacket, an electrical conductor surrounded by polymer insulation and an outer sheath, or a clad fuel rod. In these systems, the dominant pathway is radial heat conduction across dissimilar layers, so the interface conditions (continuity of temperature and heat flux) and property contrasts determine both the net thermal resistance and the local gradients that drive thermal stress and material degradation. Because many such components operate under start-up, shut-down, and cyclic environments, peak temperatures and thermal lag are set by transient, not steady, conduction. Standard heat-conduction references treat composite cylindrical media as canonical examples in which discontinuous material properties and boundary conditions shape the solution structure [1–4].

Composite-cylinder conduction models are used as basis of practical rating calculations. For high-voltage power cables, the allowable continuous current (ampacity) is set by the maximum permissible conductor and insulation temperature. Standards such as IEC 60287 compute this by treating the cable as concentric cylindrical layers and modeling heat flow outward using a thermal-resistance network: radial conduction resistances of each layer plus the external heat-transfer resistance to the surroundings [5]. In nuclear fuel rods, radial conduction through fuel and cladding, together with gap and surface heat transfer, sets peak fuel and cladding temperatures and therefore margin to safety limits. Standard reactor-thermal texts idealize the rod as a layered cylinder and emphasize the role of material properties and boundary conditions [6,7]. Layered conduction is also central in thermal protection and thermal management: thermal-barrier coatings are designed to

reduce metal temperature in hot components [8], and battery thermal-management studies highlight how temperature nonuniformity and transient loading affect performance and safety [9].

Closed-form or semi-analytical solutions are valuable for layered cylinders because they clarify how conductivity ratios, Biot numbers, and layer thicknesses shape the response. These solutions also enable rapid parametric studies without remeshing and provide benchmarks for verification. Classical heat-conduction references develop eigenfunction expansions in cylindrical coordinates and use superposition and transform ideas to treat transient boundary-value problems [1–4]. More recent syntheses continue to organize and extend analytical solutions for multilayer conduction in composite structures across geometries and boundary conditions [10–13].

Practically, the external thermal environment is rarely steady. Ambient temperature and convection conditions vary with operating cycles, weather changes, or process transients, and such forcing can be represented as periodic or general time-dependent boundary conditions. For solids subjected to periodic ambient variations, prior analyses show attenuation and phase lag between the boundary signal and internal temperatures [14]. In composite cylinders, the same dynamics couple with interfacial continuity and property contrast, so the amplitude and phase of the response can differ substantially from the homogeneous-cylinder case.

Accordingly, this paper derives an analytical solution for transient radial conduction in a two-layer composite cylinder with convection at the outer surface and a prescribed, time-dependent ambient temperature. The temperature field in each layer is represented by Bessel-function expansions, and Duhamel's principle is used to express the response to arbitrary ambient histories through a convolution in time. The general formulation is then specialized to harmonic ambient fluctuations to quantify amplitude reduction and phase shift and to recover the constant-ambient limit as the forcing frequency tends to zero. A parametric study highlights how the conductivity ratio, Biot number, and geometric aspect ratio govern interfacial gradients and mean-temperature evolution.

The Model

Consider a two-layer composite cylinder with inner radius a and outer radius b ($b > a$), initially at a uniform temperature T_0 .

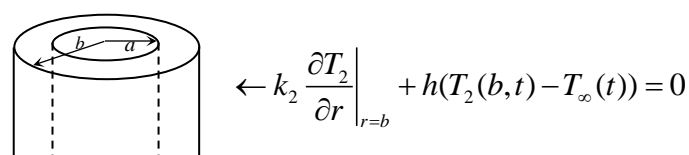


Figure 1. The Problem Configuration.

The two layers may be composed of different materials; subscripts 1 and 2 denote the inner and outer layers, respectively. Heat is exchanged with the surrounding medium by convection at the external surface. The temperature field $T(r, t)$ within the composite cylinder satisfies the transient energy equation:

$$\frac{1}{r} \frac{\partial}{\partial r} \left(r \frac{\partial T}{\partial r} \right) = \frac{1}{\alpha} \frac{\partial T}{\partial t} \quad (1)$$

where α is the thermal diffusivity, r denotes the radial distance, and t is time. The initial temperature distribution through the cylinder is given by

$$T_1(r, 0) = T_2(r, 0) = T_0 \quad (2)$$

The temperature at the center of the cylinder must remain finite, that is

$$T_1(0, t) < \infty \quad (3)$$

At the interface, both the temperature and the flux are continuous.

$$T_1(a, t) = T_2(a, t) \quad (4)$$

$$k_1 \frac{\partial T_1}{\partial r} \Big|_{r=a} = k_2 \frac{\partial T_2}{\partial r} \Big|_{r=a} \quad (5)$$

where k is the thermal conductivity. At the outer surface, convective heat exchange with the surrounding fluid is described by the boundary condition

$$-k_2 \frac{\partial T_2}{\partial r} \Big|_{r=b} = h(T_2(b, t) - T_\infty(t)) \quad (6)$$

where h is the convective heat transfer coefficient and $T_\infty(t)$ (possibly time-dependent) is the ambient fluid temperature.

We now introduce the following dimensionless variables

$$\xi = \frac{r}{b}, \quad \varepsilon = \frac{a}{b}, \quad \tau = \frac{\alpha_2}{b^2} t, \quad u = \frac{T - T_0}{T_m}, \quad Bi = hb/k_2 \quad (7)$$

where T_m is a reference temperature scale and Bi is the Biot number. With these definitions, the system (1)–(6) can be rewritten in dimensionless form as

$$\frac{\partial^2 u_1}{\partial \xi^2} + \frac{1}{\xi} \frac{\partial u_1}{\partial \xi} = \frac{\alpha_2}{\alpha_1} \frac{\partial u_1}{\partial \tau} \quad \text{and} \quad \frac{\partial^2 u_2}{\partial \xi^2} + \frac{1}{\xi} \frac{\partial u_2}{\partial \xi} = \frac{\partial u_2}{\partial \tau} \quad (8)$$

$$u_1(\xi, 0) = u_2(\xi, 0) = 0 \quad (9)$$

$$u_1(0, \tau) < \infty \quad (10)$$

$$u_1(\varepsilon, \tau) = u_2(\varepsilon, \tau) \quad (11)$$

$$k_1 \frac{\partial u_1}{\partial \xi} \Big|_{\xi=\varepsilon} = k_2 \frac{\partial u_2}{\partial \xi} \Big|_{\xi=\varepsilon} \quad (12)$$

$$\left[\frac{\partial u_2}{\partial \xi} + Bi u_2(\xi, \tau) \right]_{\xi=1} = Bi u_\infty(\tau) \quad (13)$$

To construct a solution, we first consider an auxiliary problem in which $\varphi(\xi, \tau)$ satisfies the system (8)–(13), except that the forcing term $Bi u_\infty(\tau)$ on the right-hand side of (13) is replaced by unity.

Defining $w(\xi, \tau) = \varphi(\xi, \tau) - \frac{1}{Bi}$, the system (8)–(13) can be recast in terms of $w(\xi, \tau)$ as follows:

$$\frac{\partial^2 w_1}{\partial \xi^2} + \frac{1}{\xi} \frac{\partial w_1}{\partial \xi} = \frac{\alpha_2}{\alpha_1} \frac{\partial w_1}{\partial \tau} \quad \text{and} \quad \frac{\partial^2 w_2}{\partial \xi^2} + \frac{1}{\xi} \frac{\partial w_2}{\partial \xi} = \frac{\partial w_2}{\partial \tau} \quad (14)$$

$$w_1(\xi, 0) = w_2(\xi, 0) = -\frac{1}{Bi} \quad (15)$$

$$w_1(0, \tau) < \infty \quad (16)$$

$$w_1(\varepsilon, \tau) = w_2(\varepsilon, \tau) \quad (17)$$

$$k_1 \frac{\partial w_1}{\partial \xi} \Big|_{\xi=\varepsilon} = k_2 \frac{\partial w_2}{\partial \xi} \Big|_{\xi=\varepsilon} \quad (18)$$

$$\left[\frac{\partial w_2}{\partial \xi} + Bi w_2(\xi, \tau) \right]_{\xi=1} = 0 \quad (19)$$

Equations (14) admit a separable solution, with radial eigenfunctions expressed in terms of the order-zero Bessel functions of the first and second kinds, J_0 and Y_0 . Enforcing conditions (16) and (19), and then applying (17) to the superposition, yields:

$$w_1(\xi, \tau) = \sum_{n=1}^{\infty} A_n J_0 \left(\lambda_n \sqrt{\frac{\alpha_2}{\alpha_1}} \xi \right) e^{-\lambda_n^2 \tau} \quad (20)$$

$$w_2(\xi, \tau) = \sum_{n=1}^{\infty} A_n \Omega_1 \left(J_0(\lambda_n \xi) + \Omega_0 Y_0(\lambda_n \xi) \right) e^{-\lambda_n^2 \tau} \quad (21)$$

where $\Omega_0 = \frac{\lambda_n J_1(\lambda_n) - Bi J_0(\lambda_n)}{-\lambda_n Y_1(\lambda_n) + Bi Y_0(\lambda_n)}$ and $\Omega_1 = \frac{J_0(\lambda_n \sqrt{\frac{\alpha_2}{\alpha_1}} \varepsilon)}{J_0(\lambda_n \varepsilon) + \Omega_0 Y_0(\lambda_n \varepsilon)}$.

Equation (18) is used to determine the eigenvalues λ_n ,

$$\frac{k_1}{k_2} \sqrt{\frac{\alpha_2}{\alpha_1}} J_1 \left(\lambda_n \sqrt{\frac{\alpha_2}{\alpha_1}} \varepsilon \right) - \Omega_1 \left(J_1(\lambda_n \varepsilon) + \Omega_0 Y_1(\lambda_n \varepsilon) \right) = 0 \quad (22)$$

where J_1 and Y_1 denote the first- and second-kind Bessel functions of order one, respectively. The coefficients in (20) and (21) are determined by enforcing the initial condition (15). It can be shown that

$$A_n = -\frac{1}{Bi} \frac{\frac{k_1}{\alpha_1} \int_0^\varepsilon \xi R_{1n} d\xi + \frac{k_2}{\alpha_2} \int_\varepsilon^1 \xi R_{2n} d\xi}{\frac{k_1}{\alpha_1} \int_0^\varepsilon \xi R_{1n}^2 d\xi + \frac{k_2}{\alpha_2} \int_\varepsilon^1 \xi R_{2n}^2 d\xi} \quad (23)$$

where $R_{1n}(\xi) = J_0 \left(\lambda_n \sqrt{\frac{\alpha_2}{\alpha_1}} \xi \right)$ and $R_{2n}(\xi) = \Omega_1 \left(J_0(\lambda_n \xi) + \Omega_0 Y_0(\lambda_n \xi) \right)$.

The coefficients A_n can be evaluated analytically in closed form; however, the resulting expression is lengthy, so we do not reproduce it here. Instead, an exact Mathematica command for computing A_n is provided in the Appendix.

In deriving (23), we used of the orthogonality condition:

$$\frac{k_1}{\alpha_1} \int_0^\varepsilon \xi R_{1m} R_{1n} d\xi + \frac{k_2}{\alpha_2} \int_\varepsilon^1 \xi R_{2m} R_{2n} d\xi = 0 \text{ if } n \neq m \quad (24)$$

Now, applying Duhamel's principle, the time-dependent solution can be expressed as

$$u(\xi, \tau) = \int_{\eta=0}^{\tau} Bi u_\infty(\eta) \frac{\partial \varphi(\xi, \tau - \eta)}{\partial \tau} d\eta = -Bi \int_{\eta=0}^{\tau} u_\infty(\eta) \frac{\partial w(\xi, \tau - \eta)}{\partial \eta} d\eta \quad (25)$$

This representation is valid for an arbitrary time-dependent ambient condition. The time dependence enters only through the convolution integral, which couples the exponential kernel of the eigenfunction expansion with the prescribed ambient temperature. In the special case of a constant ambient temperature ($u_\infty = \text{const.}$), the integral simplifies and the solution reduces to $Bi u_\infty \varphi(\xi, \tau)$.

Discussion

We consider an ambient temperature that varies harmonically about the composite cylinder's initial temperature:

$$T_\infty(t) = T_0 + T_m \cos(\nu_0 t) \quad (26)$$

where ν_0 is the frequency.

The corresponding dimensionless ambient temperature is

$$u_\infty(\tau) = \frac{T_\infty(\tau) - T_0}{T_m} = \cos(\omega_0 \tau) \quad (27)$$

where $\omega_0 = \frac{b^2 \nu_0}{\alpha_2}$ is the dimensionless frequency. Applying Duhamel's principle to solutions (20) and (21) then yields expressions of the form

$$u_1(\xi, \tau) = -Bi \sum_{n=1}^{\infty} A_n \lambda_n^2 J_0 \left(\sqrt{\frac{\alpha_2}{\alpha_1}} \lambda_n \xi \right) \left(\frac{-e^{-\lambda_n^2 \tau} \lambda_n^2 + \lambda_n^2 \cos(\omega_0 \tau) + \omega_0 \sin(\omega_0 \tau)}{\lambda_n^4 + \omega_0^2} \right) \quad (28)$$

$$u_2(\xi, \tau) = -Bi \sum_{n=1}^{\infty} A_n \lambda_n^2 \frac{-e^{-\lambda_n^2 \tau} \lambda_n^2 + \lambda_n^2 \cos(\omega_0 \tau) + \omega_0 \sin(\omega_0 \tau)}{\lambda_n^4 + \omega_0^2} \Omega_1 (J_0(\lambda_n \xi) + \Omega_0 Y_0(\lambda_n \xi)) \quad (29)$$

Constant Ambient Temperature:

When the frequency vanishes ($\omega_0 = 0$), the problem reduces to a composite cylinder exposed to a constant ambient temperature ($u_\infty = 1$). The corresponding solution is obtained directly from (28) and (29) by setting $\omega_0 = 0$.

We examine the influence of the conductivity ratio k_1/k_2 on the temporal evolution of the dimensionless temperature in the inner and outer layers. As noted by Alassar and Al-Attas [15], the ratios k_1/k_2 and α_1/α_2 are often comparable for commonly used metals; we adopt the same assumption here. Figure 2 presents radial profiles of the dimensionless temperature at selected dimensionless times for $Bi = 1$ and $\varepsilon = 1/2$. For small values of k_1/k_2 (Figure 2a), the inner layer offers a relatively large thermal resistance, so its temperature changes only weakly, even at later times. A pronounced "kink" appears at the interface, reflecting an abrupt change in the slope required to accommodate the discontinuity in thermal conductivity while maintaining continuity of heat flux. This kink disappears when $k_1/k_2 = 1$ (Figure 2c), corresponding to a homogeneous cylinder. For large conductivity ratios (Figure 2d), the interfacial slope change reverses sign, indicating a redistribution of the temperature gradient consistent with the higher conductivity of the inner layer.

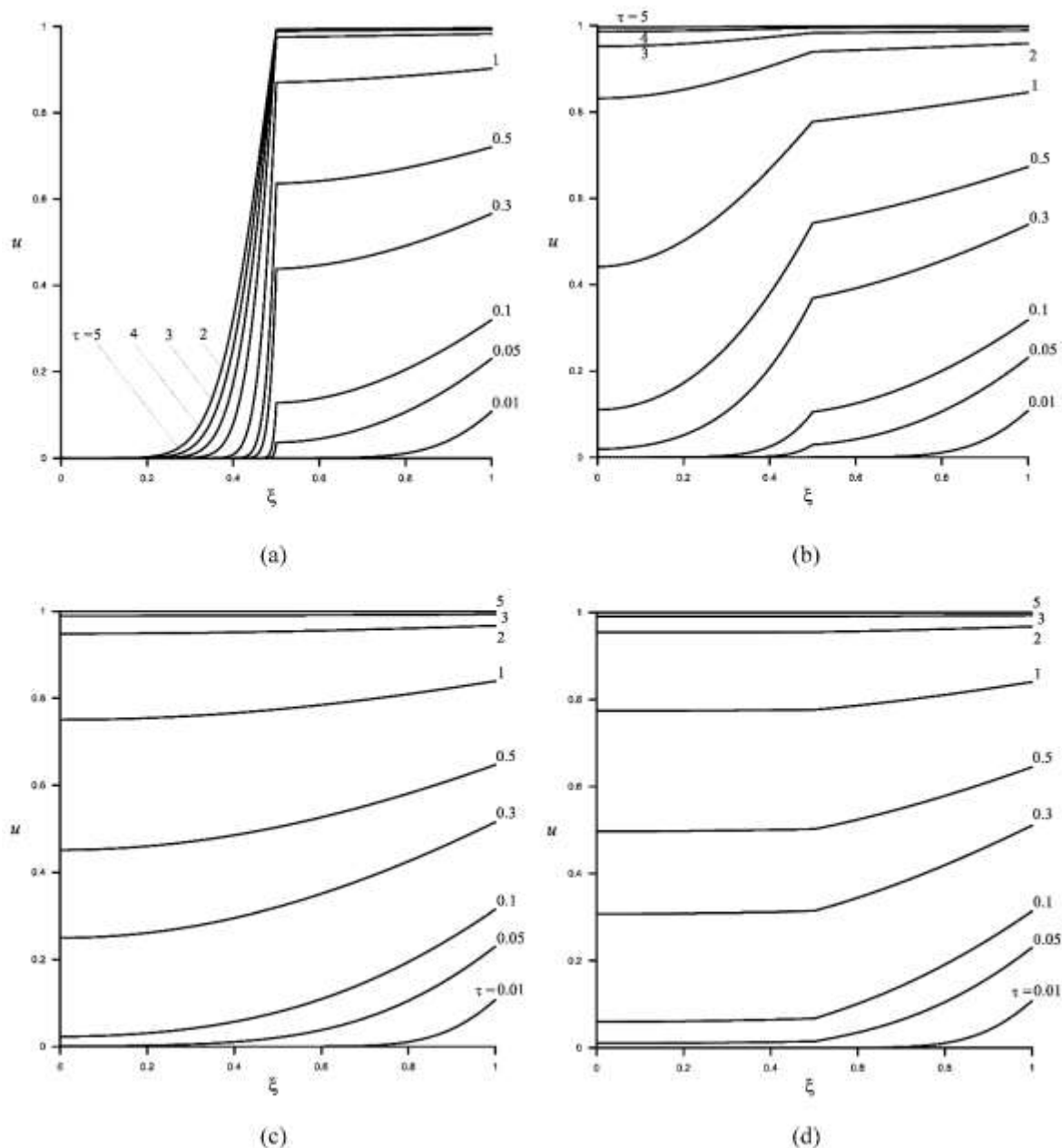


Figure 2. Dimensionless temperature along the radius for the case $Bi = 1$, $\varepsilon = 1/2$, $\omega_0 = 0$. (a) $k_1/k_2 = 0.001$ (b) $k_1/k_2 = 0.1$ (c) $k_1/k_2 = 1$ (d) $k_1/k_2 = 10$.

Figure 3a indicates that, for small conductivity ratios, the transient evolution of the average dimensionless temperature is sensitive to k_1/k_2 . However, once k_1/k_2 exceeds roughly 0.1, the response becomes only weakly dependent on further increases in conductivity ratio. In this regime, the thermal behavior is governed primarily by the outer layer (the annulus), and the curves nearly collapse for $k_1/k_2 \geq 1$.

The limiting case $k_1/k_2 \rightarrow \infty$ (also shown in Figure 3a) yields the fastest heat-transfer rate. At the other extreme, $k_1/k_2 \rightarrow 0$ represents a lower bound in which the interface effectively behaves as an insulated boundary for the annulus. This may be modeled by replacing condition (12) with $\frac{\partial u_2}{\partial \xi} \Big|_{\xi=\varepsilon} = 0$. A closed-form solution for this special case is provided in the Appendix.

Figure 3b illustrates the influence of the Biot number on heat transfer. As Bi increases, the heat-transfer rate increases but approaches an upper limit. This limiting behavior, corresponding to $Bi \rightarrow \infty$, is also derived in the Appendix. Physically, $Bi \rightarrow \infty$ implies an isothermal outer surface, i.e., a Dirichlet boundary condition obtained by replacing (13) with $u_2(1, \tau) = u_\infty(\tau)$.

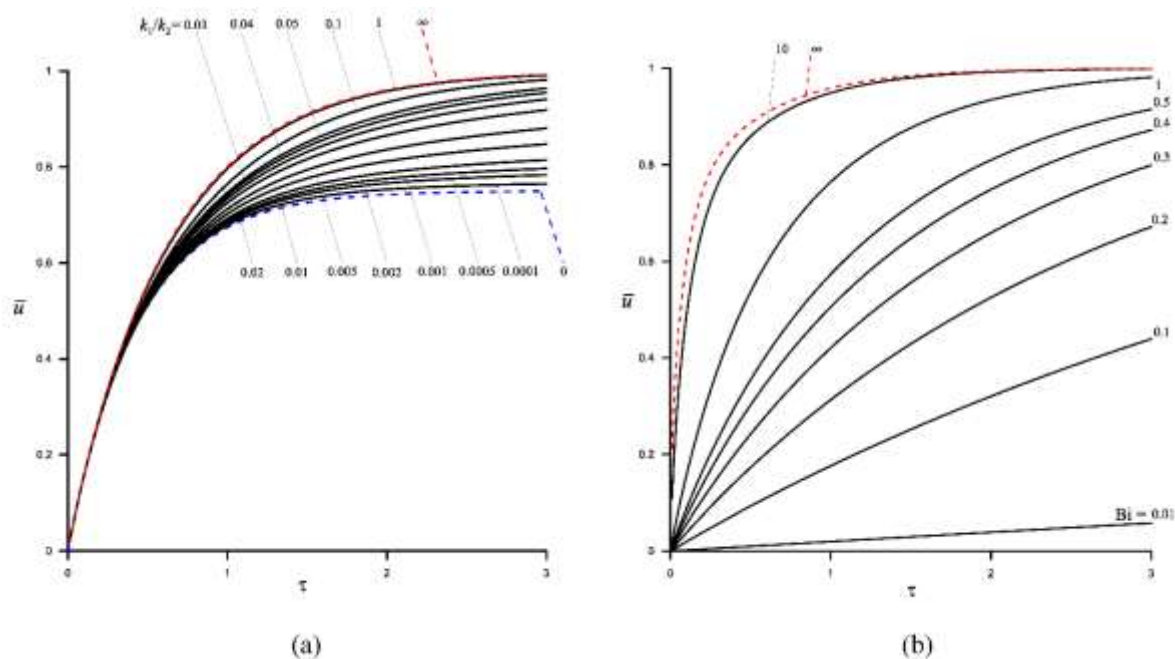


Figure 3. Development of the average temperature for $\varepsilon = \frac{1}{2}$, (a) $Bi = 1$, (b) $k_1/k_2 = 0.1$.

The average dimensionless temperature of the composite cylinder is calculated by

$$\bar{u}(\tau) = 2 \left(\int_0^\varepsilon \xi u_1 d\xi + \int_\varepsilon^1 \xi u_2 d\xi \right) \quad (30)$$

Figure 4 illustrates the influence of the aspect ratio ε on the temporal evolution of $\bar{u}(\tau)$ for several values of k_1/k_2 . In Figure 4a, ε is chosen as $\sqrt[3]{\frac{1}{10}}$, $\sqrt[3]{\frac{2}{10}}$, ..., $\sqrt[3]{\frac{9}{10}}$ so that the two regions partition the (normalized) domain into equal-volume increments.

For small k_1/k_2 , the inner layer offers a large thermal resistance, and decreasing ε (i.e., reducing the inner-layer thickness) leads to a faster overall heat-transfer rate. As k_1/k_2 approaches unity, the sensitivity to ε , as expected, diminishes. When $k_1 = k_2$, the cylinder behaves as a single homogeneous material and the interface location becomes immaterial. When $k_1/k_2 > 1$, the trend reverses (though the effect is comparatively quite modest): smaller ε corresponds to a slightly slower heat-transfer rate.

A particularly relevant limiting case is $\varepsilon \rightarrow 1$, which models an extremely thin outer coating. Spray-on coatings are typically thinner than 1 mm and often have thermal conductivities in the range 0.04 – 0.08 W/m.K, whereas common metals such as gold, copper, steel, and aluminum have conductivities on the order of 40-500 W/m.K [16–18]. The resulting conductivity ratio k_1/k_2 therefore ranges from $\mathcal{O}(10^2)$ to above $\mathcal{O}(10^4)$. Since we have shown that, for $k_1/k_2 > 1$, the evolution of $\bar{u}(\tau)$ becomes largely insensitive to further increases in k_1/k_2 , it is reasonable over this range to assume that $k_1/k_2 \rightarrow \infty$.

Figure 5 presents $\bar{u}(\tau)$ for the limiting case $\varepsilon \rightarrow 1$ and $k_1/k_2 \rightarrow \infty$ under different Biot numbers. These curves quantify the transient response of a cylinder coated with an extremely thin, low-conductivity layer.

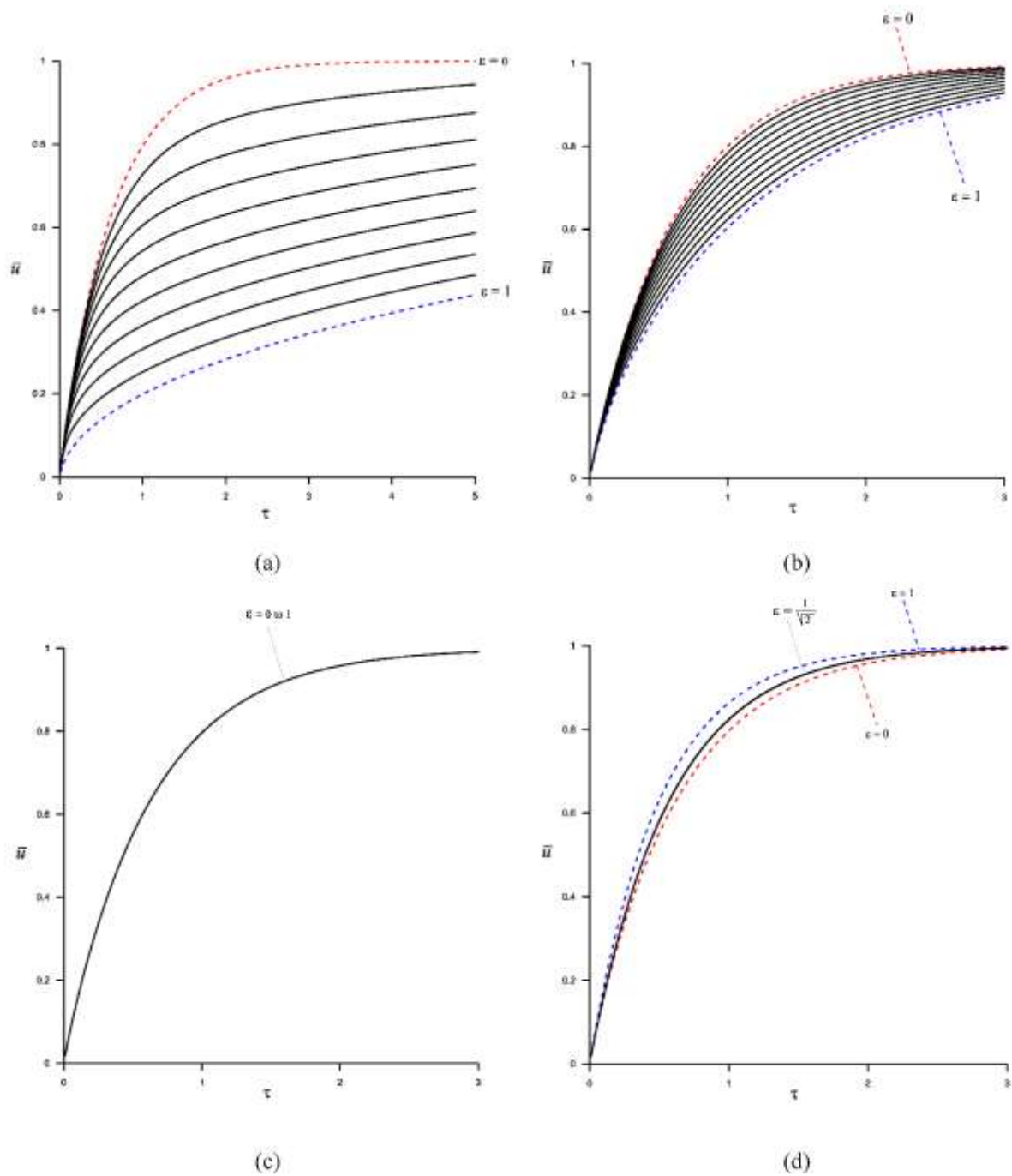


Figure 4. Impact of aspect ratio on the average dimensionless temperature, $Bi = 1$. (a) $k_1/k_2 = 0.01$ (b) $k_1/k_2 = 0.2$ (c) $k_1/k_2 = 1$ (d) $k_1/k_2 = 100$.

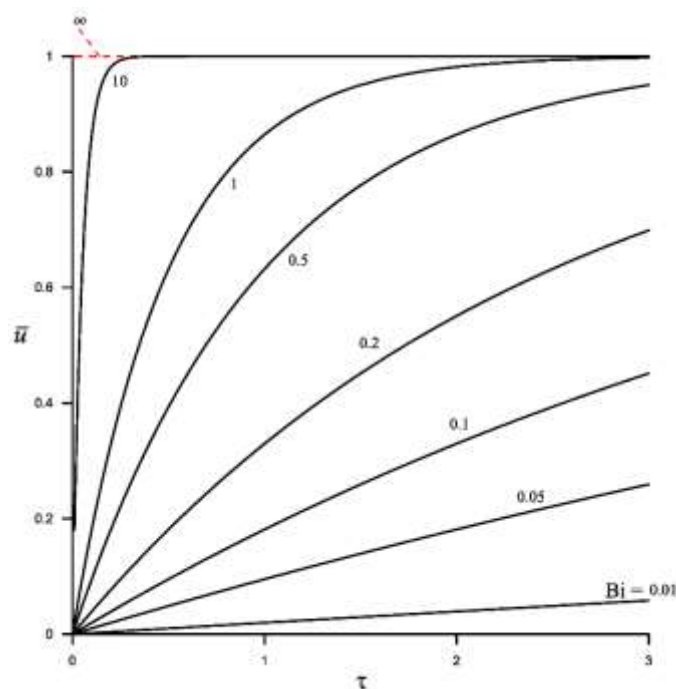


Figure 5. Average dimensionless temperature, $\varepsilon \rightarrow 1$ and $k_1/k_2 \rightarrow \infty$.

Harmonically Fluctuating Ambient Temperature:

The dimensionless temperature field under a harmonically fluctuating ambient condition can be evaluated directly from solutions (28) and (29). Figure 6 presents radial profiles of the dimensionless temperature at several instants over a single period. The results show that the start-up transients decay after only a few cycles; in the example shown, a quasi-steady state is essentially established by the fifth cycle. The case considered corresponds to $k_1/k_2 = 0.1$, $Bi = 1$, and $\varepsilon = 3/4$, with frequencies $\omega_0 = \pi/2$ and $\omega_0 = 2\pi$. At the lower frequency, the thermal oscillations penetrate more deeply into the composite cylinder and exhibit a larger amplitude.

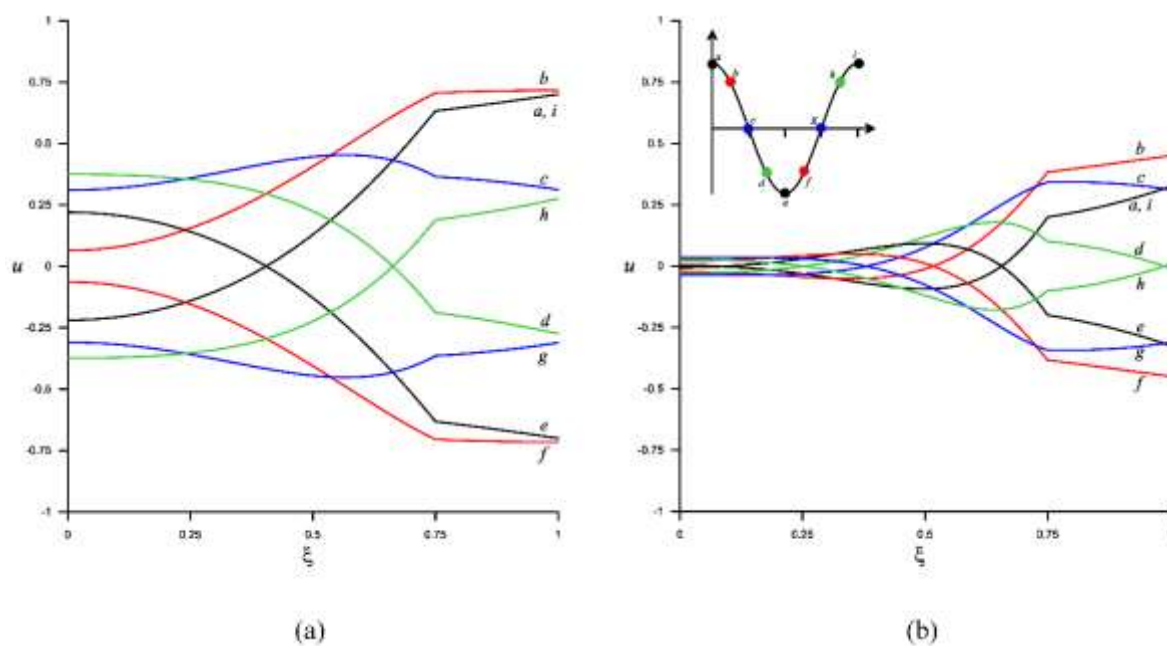


Figure 6. Development of the dimensionless temperature $k_1/k_2 = 0.1$, $Bi = 1$, $\varepsilon = 3/4$. (a) $\omega_0 = \pi/2$, (b) $\omega_0 = 2\pi$.

To facilitate comparison among different frequencies, we normalize the cycle length by introducing the variable $\tau^* = \frac{\tau}{2\pi/\omega_0}$ so that one full cycle has a unit period length. We focus on the quasi-steady (periodic) regime, i.e., after the initial transients have decayed over a few cycles. Figure 7 shows the evolution of the average dimensionless temperature \bar{u} over the fifth cycle for $k_1/k_2 = 10$, $Bi = 1$, and $\varepsilon = 1/2$. As the frequency increases, the normalized phase lag becomes more pronounced and the oscillation amplitude decreases. The influence of Biot number on both the amplitude and phase lag is illustrated in Figure 8 for $k_1/k_2 = 1$, $\omega_0 = \pi/4$, and $\varepsilon = 1/2$. The limiting solution for very large Bi is provided in the Appendix. As Bi increases, the amplitude of \bar{u} increases, as expected, and the thermal response becomes more immediate, i.e., the phase lag relative to the ambient oscillations is reduced.

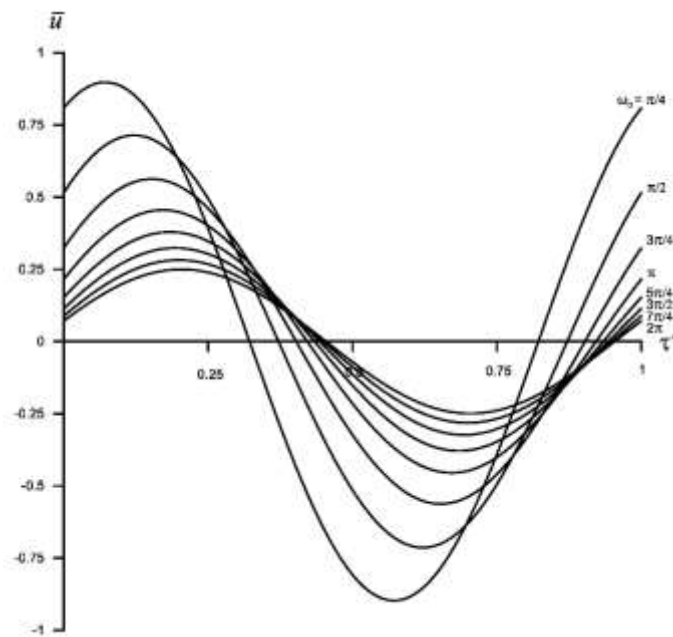


Figure 7. : Average dimensionless temperature over a cycle, $k_1/k_2 = 10$, $Bi = 1$, $\varepsilon = 1/2$.

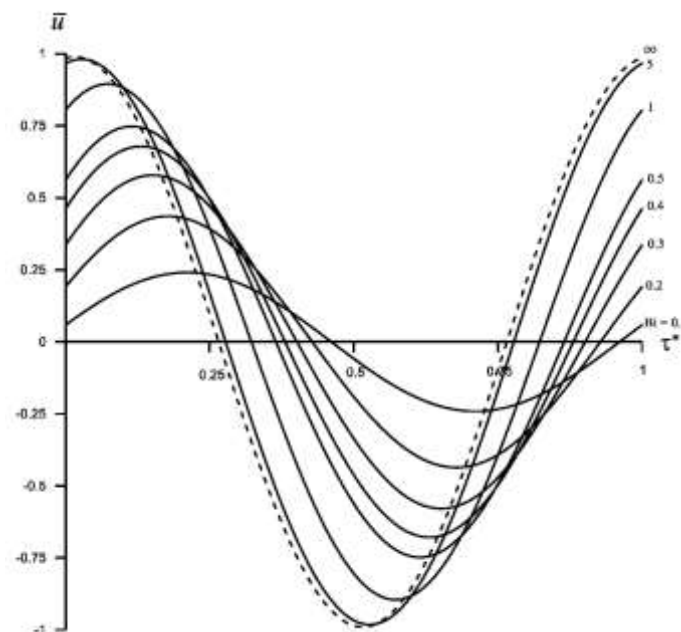


Figure 8. : Average dimensionless temperature over a cycle, $k_1/k_2 = 1$, $\omega_0 = \pi/4$, $\varepsilon = 1/2$.

Figure 9 compares the average dimensionless temperature response for different aspect ratios ε . For large conductivity ratios ($k_1/k_2 \gg 1$), variations in ε produce no noticeable change across the Biot numbers considered. In this regime, increasing Bi primarily amplifies the response and reduces the phase lag (e.g., compare Figure 9b with 9d, or Figure 9a with 9c). In contrast, when $k_1/k_2 \ll 1$, the aspect ratio influences both the amplitude and the phase of \bar{u} . As shown in Figure 9a, increasing ε increases the relative influence of the low-conductivity inner layer, which slows the thermal response and results in larger delays and more pronounced phase shifts relative to the ambient fluctuations.

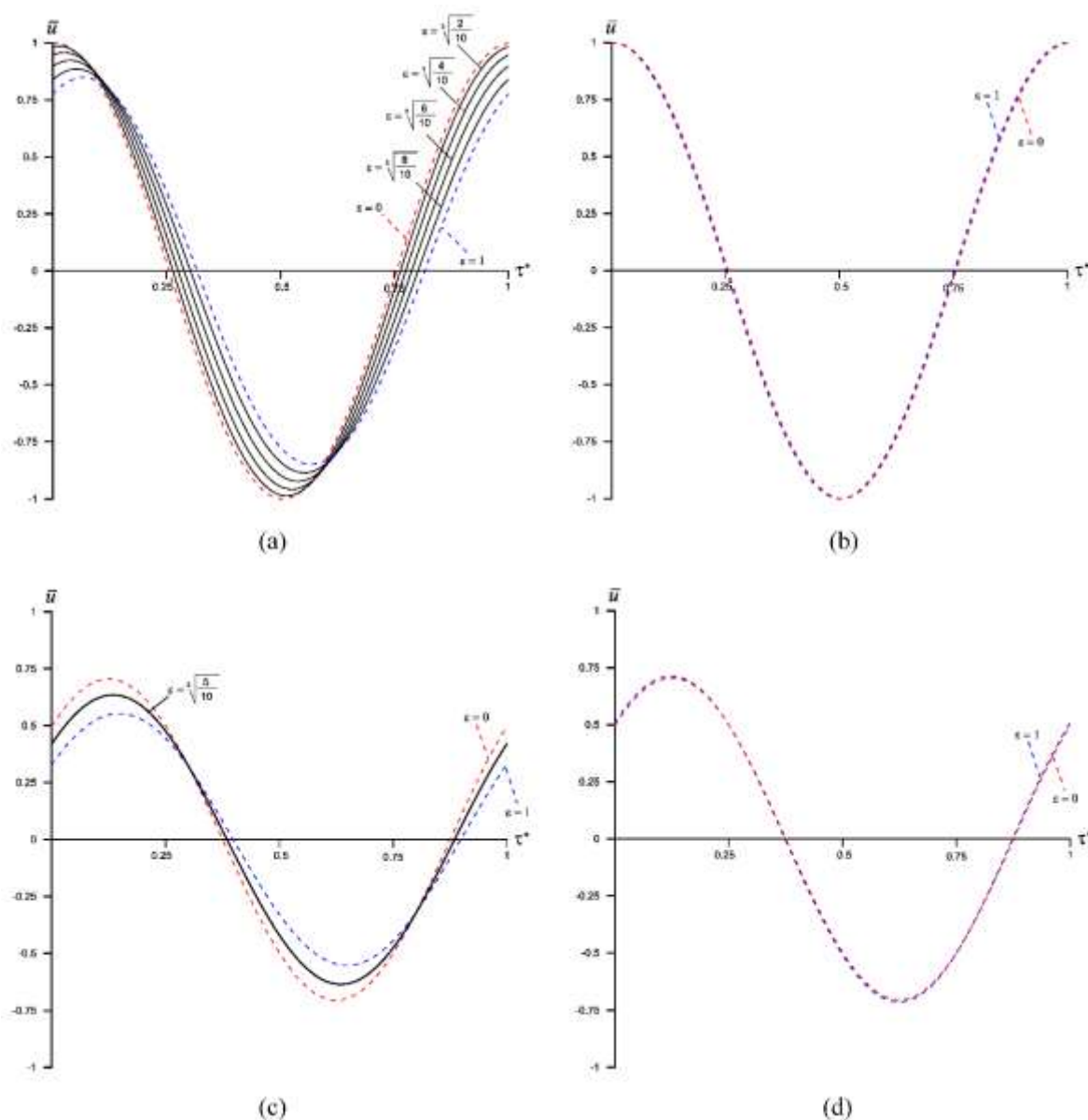


Figure 9. Average dimensionless temperature over a cycle, $\omega_0 = \pi/16$. (a) $Bi = 10$, $\frac{k_1}{k_2} = 0.05$, (b) $Bi = 10$, $\frac{k_1}{k_2} = 20$, (c) $Bi = 0.1$, $\frac{k_1}{k_2} = 0.05$, (d) $Bi = 0.1$, $\frac{k_1}{k_2} = 20$.

Conclusions

We presented an analytical solution for transient heat conduction in a two-layer composite cylinder subject to convection at the outer surface with a time-dependent ambient temperature. Using

expansions in terms of Bessel functions and invoking Duhamel's principle, we derived closed-form expressions for the dimensionless temperatures in the inner and outer layers. These expressions are valid for a general time-dependent boundary condition. We specialized the general solution to the case where the ambient temperature varies harmonically about the initial temperature. The expressions reduce, in the limiting case as the frequency $\omega_0 \rightarrow 0$, to the classical constant-ambient problem ($u_\infty = 1$).

A parametric investigation clarified how material and boundary parameters control the transient thermal responses. For constant ambient conditions, the conductivity ratio k_1/k_2 strongly affects the radial temperature gradients and produces a distinct interfacial "kink" when the conductivities differ, consistent with continuity of heat flux. The average dimensionless temperature is sensitive to k_1/k_2 only for small ratios; once $k_1/k_2 \gtrsim 0.1$, the evolution becomes largely governed by the outer annulus and changes little for $k_1/k_2 \geq 1$. The limiting bounds $k_1/k_2 \rightarrow 0$ (effectively insulated interface for the annulus) and $k_1/k_2 \rightarrow \infty$ (fastest transfer) were identified, with supporting closed-form developments provided in the Appendix. Similarly, increasing the Biot number accelerates heat transfer but approaches an upper bound as $Bi \rightarrow \infty$, corresponding to an isothermal outer surface (Dirichlet condition).

The aspect ratio $\varepsilon = a/b$ plays an important role when the inner layer is resistive ($k_1/k_2 \ll 1$), where reducing ε generally enhances the heat-transfer rate. Its influence diminishes as $k_1/k_2 \rightarrow 1$ and becomes quite weak for $k_1/k_2 \gg 1$. A practically important regime is when $\varepsilon \rightarrow 1$, representing extremely thin coatings. For typical low-conductivity coatings on highly conductive metals, k_1/k_2 is very large, and our results justify the approximation $k_1/k_2 \rightarrow \infty$; the corresponding $\bar{u}(\tau)$ response under different Biot numbers quantifies the thermal "shielding" effect of thin insulating layers.

Under harmonic fluctuations of the ambient conditions, the solution transitions rapidly to a periodic steady state after only a few cycles. Frequency primarily controls thermal penetration, amplitude, and phase lag: lower ω_0 produces deeper penetration and larger oscillation amplitudes, whereas increasing ω_0 attenuates the response and increases the phase lag. The Biot number amplifies the oscillation amplitude and reduces the phase delay, yielding a more immediate tracking of ambient fluctuations. Finally, the coupling between ε and k_1/k_2 governs the dynamic response: when $k_1/k_2 \gg 1$, ε has little effect, but when $k_1/k_2 \ll 1$, increasing ε strengthens the influence of the low-conductivity inner layer and produces substantial delays and larger phase shifts.

Acknowledgments: The author would like to acknowledge King Fahd University of Petroleum & Minerals (KFUPM) for supporting this research.

Appendix

The general problem under consideration in dimensionless form is that described by equations (8-13). We consider the following limiting/special cases.

A) The Case $Bi \rightarrow \infty$

The only change is in equation (13) in the general system. The system may be rewritten as

$$\frac{\partial^2 u_1}{\partial \xi^2} + \frac{1}{\xi} \frac{\partial u_1}{\partial \xi} = \frac{\alpha_2}{\alpha_1} \frac{\partial u_1}{\partial \tau} \quad (\text{A1})$$

$$\frac{\partial^2 u_2}{\partial \xi^2} + \frac{1}{\xi} \frac{\partial u_2}{\partial \xi} = \frac{\partial u_2}{\partial \tau} \quad (\text{A2})$$

$$u_1(\xi, 0) = u_2(\xi, 0) = 0 \quad (\text{A3})$$

$$u_1(0, \tau) < \infty \quad (\text{A4})$$

$$u_1(\varepsilon, \tau) = u_2(\varepsilon, \tau) \quad (\text{A5})$$

$$k_1 \left. \frac{\partial u_1}{\partial \xi} \right|_{\xi=\varepsilon} = k_2 \left. \frac{\partial u_2}{\partial \xi} \right|_{\xi=\varepsilon} \quad (\text{A6})$$

$$u_2(1, \tau) = u_\infty(\tau) \quad (\text{A7})$$

Let $\varphi(\xi, \tau)$ be the solution for the system with the right-hand side of equation (A7) set to 1. Following the same procedure, one can show that

$$\varphi_1(\xi, \tau) = 1 + \sum_{n=1}^{\infty} A_n J_0\left(\sqrt{\frac{\alpha_2}{\alpha_1}} \lambda_n \xi\right) e^{-\lambda_n^2 \tau} \quad (\text{A8})$$

$$\varphi_2(\xi, \tau) = 1 + \sum_{n=1}^{\infty} A_n \psi_1 [J_0(\lambda_n \xi) + \psi_0 Y_0(\lambda_n \xi)] e^{-\lambda_n^2 \tau} \quad (\text{A9})$$

where $\psi_0 = -\frac{J_0(\lambda_n)}{Y_0(\lambda_n)}$ and $\psi_1 = \frac{J_0\left(\sqrt{\frac{\alpha_2}{\alpha_1}} \lambda_n \varepsilon\right)}{J_0(\lambda_n \varepsilon) + \Omega_0 Y_0(\lambda_n \varepsilon)}$. The coefficients A_n are given by

$$A_n = -\frac{\frac{k_1}{\alpha_1} \int_0^\varepsilon \xi R_{1n} d\xi + \frac{k_2}{\alpha_2} \int_\varepsilon^1 \xi R_{2n} d\xi}{\frac{k_1}{\alpha_1} \int_0^\varepsilon \xi R_{1n}^2 d\xi + \frac{k_2}{\alpha_2} \int_\varepsilon^1 \xi R_{2n}^2 d\xi} \quad (\text{A10})$$

where $R_{1n}(\xi) = J_0\left(\lambda_n \sqrt{\frac{\alpha_2}{\alpha_1}} \xi\right)$ and $R_{2n}(\xi) = \psi_1 [J_0(\lambda_n \xi) + \psi_0 Y_0(\lambda_n \xi)]$. The expression for A_n is easily calculated in closed form. We use (A6) to determine the eigenvalues λ_n ,

$$\frac{k_1}{k_2} \sqrt{\frac{\alpha_2}{\alpha_1}} J_1\left(\lambda_n \sqrt{\frac{\alpha_2}{\alpha_1}} \varepsilon\right) - \psi_1 (J_1(\lambda_n \varepsilon) + \psi_0 Y_1(\lambda_n \varepsilon)) = 0 \quad (\text{A11})$$

Using Duhamel's principle, the solution is

$$u(\xi, \tau) = \int_{\eta=0}^{\tau} u_{\infty}(\eta) \frac{\partial \varphi(\xi, \tau - \eta)}{\partial \tau} d\eta \quad (\text{A12})$$

B) The Case $\varepsilon = 0$

In this case, the general system reduces to

$$\frac{\partial^2 u_2}{\partial \xi^2} + \frac{1}{\xi} \frac{\partial u_2}{\partial \xi} = \frac{\partial u_2}{\partial \tau} \quad (\text{B1})$$

$$u_2(\xi, 0) = 0 \quad (\text{B2})$$

$$u_2(0, \tau) < \infty \quad (\text{B3})$$

$$\left[\frac{\partial u_2}{\partial \xi} + Bi u_2(\xi, \tau) \right]_{\xi=1} = Bi u_{\infty}(\tau) \quad (\text{B4})$$

Let $\varphi_2(\xi, \tau)$ be the solution for the system with the right-hand side of equation (B4) set to 1.

Following the same procedure, one can show that

$$\varphi_2(\xi, \tau) = \frac{1}{Bi} + \sum_{n=1}^{\infty} A_n J_0(\lambda_n \xi) e^{-\lambda_n^2 \tau} \quad (\text{B5})$$

$$A_n = \frac{-2 J_1(\lambda_n)}{Bi \lambda_n (J_0^2(\lambda_n) + J_1^2(\lambda_n))} \quad (\text{B6})$$

The eigenvalues are determined by

$$-\lambda_n J_1(\lambda_n) + Bi J_0(\lambda_n) = 0 \quad (\text{B7})$$

C) The Case $\varepsilon = 1$

In this case, the general system reduces to

$$\frac{\partial^2 u_1}{\partial \xi^2} + \frac{1}{\xi} \frac{\partial u_1}{\partial \xi} = \frac{\alpha_2}{\alpha_1} \frac{\partial u_1}{\partial \tau} \quad (\text{C1})$$

$$u_1(\xi, 0) = 0 \quad (\text{C2})$$

$$u_1(0, \tau) < \infty \quad (\text{C3})$$

$$\left[\frac{\partial u_1}{\partial \xi} + \frac{k_2}{k_1} Bi u_1(\xi, \tau) \right]_{\xi=1} = \frac{k_2}{k_1} Bi u_{\infty}(\tau) \quad (\text{C4})$$

This equivalent to Case B except for the scaling by α_2 in (C1).

Let $\varphi_1(\xi, \tau)$ be the solution for the system with the right-hand side of equation (C4) set to 1.

Following the same procedure, one can show that

$$\varphi_1(\xi, \tau) = \frac{1}{\frac{k_2}{k_1} Bi} + \sum_{n=1}^{\infty} A_n J_0\left(\sqrt{\frac{\alpha_2}{\alpha_1}} \lambda_n \xi\right) e^{-\lambda_n^2 \tau} \quad (\text{C5})$$

$$A_n = \frac{-2 J_1(\sqrt{\frac{\alpha_2}{\alpha_1}} \lambda_n)}{\frac{k_2}{k_1} Bi \lambda_n \sqrt{\frac{\alpha_2}{\alpha_1}} (J_0^2(\sqrt{\frac{\alpha_2}{\alpha_1}} \lambda_n) + J_1^2(\sqrt{\frac{\alpha_2}{\alpha_1}} \lambda_n))} \quad (\text{C6})$$

The eigenvalues are determined by

$$-\lambda_n \sqrt{\frac{\alpha_2}{\alpha_1}} J_1\left(\sqrt{\frac{\alpha_2}{\alpha_1}} \lambda_n\right) + \frac{k_2}{k_1} Bi J_0\left(\sqrt{\frac{\alpha_2}{\alpha_1}} \lambda_n\right) = 0 \quad (\text{C7})$$

Using Duhamel's principle, the solution is

$$u(\xi, \tau) = \int_{\eta=0}^{\tau} \frac{k_2}{k_1} Bi u_{\infty}(\eta) \frac{\partial \varphi(\xi, \tau - \eta)}{\partial \tau} d\eta \quad (\text{C8})$$

D) The Case $\frac{k_1}{k_2} \rightarrow 0$

In this case, the interface works as an insulator and the general system reduces to

$$\frac{\partial^2 u_2}{\partial \xi^2} + \frac{1}{\xi} \frac{\partial u_2}{\partial \xi} = \frac{\partial u_2}{\partial \tau} \quad (D1)$$

$$u_2(\xi, 0) = 0 \quad (D2)$$

$$\left. \frac{\partial u_2}{\partial \xi} \right|_{\xi=\varepsilon} = 0 \quad (D3)$$

$$\left[\frac{\partial u_2}{\partial \xi} + Bi u_2(\xi, \tau) \right]_{\xi=1} = Bi u_\infty(\tau) \quad (D4)$$

Let $\varphi_2(\xi, \tau)$ be the solution for the system with the right-hand side of equation (D4) set to 1.

Following the same procedure, one can show that

$$\varphi_2(\xi, \tau) = \frac{1}{Bi} + \sum_{n=1}^{\infty} A_n R_n(\xi) e^{-\lambda_n^2 \tau} \quad (D5)$$

where $R_n(\xi) = J_0(\lambda_n \xi) + \frac{-Bi J_0(\lambda_n) + \lambda_n J_1(\lambda_n)}{Bi Y_0(\lambda_n) - \lambda_n Y_1(\lambda_n)} Y_0(\lambda_n \xi)$, and A_n are found by

$$A_n = \frac{-1 \int_{\varepsilon}^1 \xi R_n(\xi) d\xi}{Bi \int_{\varepsilon}^1 \xi R_n^2(\xi) d\xi} \quad (D6)$$

The eigenvalues are determined by

$$J_1(\lambda_n \varepsilon) + \frac{-Bi J_0(\lambda_n) + \lambda_n J_1(\lambda_n)}{Bi Y_0(\lambda_n) - \lambda_n Y_1(\lambda_n)} Y_1(\lambda_n \varepsilon) = 0 \quad (D7)$$

Using Duhamel's principle, the solution is

$$u(\xi, \tau) = \int_{\eta=0}^{\tau} Bi u_\infty(\eta) \frac{\partial \varphi(\xi, \tau - \eta)}{\partial \tau} d\eta \quad (D8)$$

E) Mathematica commands to evaluate the coefficients

$$\Omega_0 = (\delta * \text{BesselJ}[1, \delta] - \text{Bi} * \text{BesselJ}[0, \delta]) / ((-\delta) * \text{BesselY}[1, \delta] + \text{Bi} * \text{BesselY}[0, \delta]);$$

$$\Omega_1 = \text{BesselJ}[0, \text{Sqrt}[\alpha_2 / \alpha_1] * \delta * \varepsilon] / (\text{BesselJ}[0, \delta * \varepsilon] + \Omega_0 * \text{BesselY}[0, \delta * \varepsilon]);$$

$$R_1 = \text{BesselJ}[0, \text{Sqrt}[\alpha_2 / \alpha_1] * \delta * \xi];$$

$$R_2 = \Omega_1 * (\text{BesselJ}[0, \delta * \xi] + \Omega_0 * \text{BesselY}[0, \delta * \xi]);$$

$$(\text{Integrate}[\xi * R_1, \{\xi, 0, \varepsilon\}] + (k_2 / (k_1 * (\alpha_2 / \alpha_1))) * \text{Integrate}[\xi * R_2, \{\xi, \varepsilon, 1\}]) / (\text{Integrate}[\xi * R_1^2, \{\xi, 0, \varepsilon\}] + (k_2 / (k_1 * (\alpha_2 / \alpha_1))) * \text{Integrate}[\xi * R_2^2, \{\xi, \varepsilon, 1\}])$$

References

1. H. S. Carslaw and J. C. Jaeger, *Conduction of Heat in Solids*, 2nd ed. Oxford, UK: Oxford University Press, 1959.
2. M. N. Ozisik, *Heat Conduction*, 2nd ed. New York, NY, USA: John Wiley & Sons, 1993.
3. J. Crank, *The Mathematics of Diffusion*, 2nd ed. Oxford, UK: Oxford University Press, 1975.
4. F. P. Incropera, D. P. DeWitt, T. L. Bergman, and A. S. Lavine, *Fundamentals of Heat and Mass Transfer*, 7th ed. Hoboken, NJ, USA: Wiley, 2011.
5. International Electrotechnical Commission, 2023, *Electric cables—Calculation of the current rating—Part 1-1: Current rating equations (100% load factor) and calculation of losses—General*, IEC 60287-1-1:2023, Ed. 3.0, May 22, 2023.
6. Todreas, N. E., and Kazimi, M. S., 2021, *Nuclear Systems, Volume I: Thermal Hydraulic Fundamentals*, 3rd ed., CRC Press, Boca Raton, FL.
7. Duderstadt, J. J., and Hamilton, L. J., 1976, *Nuclear Reactor Analysis*, John Wiley & Sons, New York, NY.
8. Padture, N. P., Gell, M., and Jordan, E. H., 2002, "Thermal Barrier Coatings for Gas-Turbine Engine Applications," *Science*, 296(5566), pp. 280–284, doi:10.1126/science.1068609.
9. Wang, Q., Jiang, B., Li, B., and Yan, Y., 2016, "A Critical Review of Thermal Management Models and Solutions of Lithium-Ion Batteries for the Development of Pure Electric Vehicles," *Renew. Sustain. Energy Rev.*, 64, pp. 106–128, doi:10.1016/j.rser.2016.05.033.
10. Amiri Delouei, A., Emamian, A., Sajjadi, H., Atashafrooz, M., Li, Y., Wang, L.-P., Jing, D., and Xie, G., 2021, "A Comprehensive Review on Multi-Dimensional Heat Conduction of Multi-Layer and Composite Structures: Analytical Solutions," *J. Therm. Sci.*, 30(6), pp. 1875–1907, doi:10.1007/s11630-021-1517-1.
11. Keifari Kheibari, A., Jafari, M., and Nazari, M. B., 2020, "Propagation of Heat Wave in Composite Cylinder Using Cattaneo-Vernotte Theory," *Int. J. Heat Mass Transfer*, 160, p. 120208. doi: 10.1016/j.ijheatmasstransfer.2020.120208.

12. Atefi, G., Abdous, M. A., and Ganjehkaviri, A., 2008, "Analytical Solution of Temperature Field in Hollow Cylinder under Time Dependent Boundary Condition Using Fourier series," *American Journal of Engineering and Applied Sciences*, Vol. 1, No. 2, pp. 141–148, doi:10.3844/ajeassp.2008.141.148.
13. Najibi, A., and Wang, G.-H., 2023, "Two-Dimensional C-V Heat Conduction Investigation of an FG-Finite Axisymmetric Hollow Cylinder," *Symmetry*, Vol. 15, No. 5, Art. No. 1009, doi:10.3390/sym15051009.
14. Zhang, Y., and Chen, Z., 2008, "Transient Heat Conduction in Solids Subjected to Periodic Ambient Temperature," *Int. J. Therm. Sci.*, 47, pp. 102–110.
15. Alassar, R. S., and Al-Attas, H., 2025, "On the Lump Model in a Composite Sphere," *J. Heat Mass Transfer*, 147(12), Art. No. 124501. doi:10.1115/1.4069193.
16. Y. S. Touloukian, Thermophysical Properties of Matter: The TPRC Data Series, Volume 1-10. Purdue University, 1970.
17. APA (7th edition): ASM International. (n.d.). Thermal Conductivity of Metals and Alloys. In ASM Handbook. ASM Digital Library. <https://dl.asminternational.org/handbooks/edited-volume/57/chapter/671290/Thermal-Conductivity-of-Metals-and-Alloys>.
18. L. I. Martynenko and V. P. Skripov, Handbook of Thermophysical Properties of Metals at High Temperatures. Hemisphere Publishing, 1980.

Disclaimer/Publisher's Note: The statements, opinions and data contained in all publications are solely those of the individual author(s) and contributor(s) and not of MDPI and/or the editor(s). MDPI and/or the editor(s) disclaim responsibility for any injury to people or property resulting from any ideas, methods, instructions or products referred to in the content.